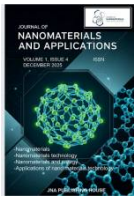
JOURNAL OF NANOMATERIALS AND APPLICATIONS

Journal of Nanomaterials and Applications



Nanomagnetic Materials: Fundamental Physics, Fabrication Strategies, and Emerging Applications

Dung Nguyen Trong[1,*], Ştefan Ţălu [2], Aurelian Sipos [3], Niranjan Patra [4], Deniz Şahin [5], Nesrine Haddad [6], Chandra Kumar [7], Claudio Larosa [8], Alia Méndez-Albores [9]

[1] Faculty of Applied Sciences, University of Transport Technology, 54 Trieu Khuc, 100000, Hanoi, Vietnam.

[2] The Directorate of Research, Development and Innovation Management (DMCDI), Technical University of Cluj-Napoca, 15 Constantin Daicoviciu St., Cluj-Napoca, 400020, Cluj county, Romania.

[3] International College, Brighton College, Eastern Road, Brighton, East Sussex BN2 0AL, United Kingdom.

[4] Department of Chemistry, Koneru Lakshmaiah Education Foundation, Greenfield, Vaddeswaram, Andhra Pradesh 522502, India.

[5] Department of Chemistry, Faculty of Science, Gazi University, 06560 Teknikokullar Yenimahalle/Ankara, Turkey.

[6] Laboratory of Physics of Materials and Nanomaterials Applied at Environment (LaPhyMNE), Faculty of Sciences in Gabes, Gabes University, 6072 Gabes, Tunisia.

7 School of Engineering, Faculty of Sciences, Engineering and Technology, Universidad Mayor, Santiago 7500994, Chile.

[8] ENEA – Energy Technologies and Renewable Sources Department (TERIN), ENEA Research Center, Via Anguillarese 301, 00123 Santa Maria di Galeria, Rome, Italy

[9] Department of Zeolite Research, Postgraduate Program in Environmental Sciences, Benemérita Universidad Autónoma de Puebla, University City, C.P. 72530, Puebla, Mexico.

Review info

Type of articles:

Review article

Abstract: This review systematizes the evolution of magnetic materials from conventional ferromagnets to multifunctional nanostructures and emerging quantum systems. We analyze the interplay between nanoscale confinement, interfacial exchange coupling, and surface spin disorder governing key phenomena—superparamagnetism, exchange bias, magnetic anisotropy, and giant/tunnelling magnetoresistance (GMR/TMR) integrating

Corresponding author*:
Dung Nguyen Trong:
dungnt78@utt.edu.vn

Received: 07 October 2026
Revised: 14 November 2026
Accepted: 15 November 2026
Published: 28 November 2026

Néel–Brown relaxation, micromagnetic theory, and atomistic Monte Carlo simulations. By critically comparing wet-chemical synthesis with physical and chemical thin-film deposition techniques, we elucidate how crystallographic and interfacial engineering tailors magnetic performance. Emphasis is placed on breakthrough frontiers (2020–2026), including spintronics (SOT-MRAM, neuromorphic computing), magnetic skyrmions, 2D van der Waals magnets, altermagnetism, precision biomedicine (hyperthermia, dual-mode MRI, targeted delivery), environmental remediation, and magnetocaloric cooling. Finally, we address critical challenges in scalability, biosafety, rare-earth dependency, and device integration, highlighting machine learning-accelerated discovery toward commercialization.

Keywords: 2D van der Waals magnets; Exchange bias; Magnetic anisotropy; Magnetic hyperthermia; Magnetic skyrmions; Nanomagnetic materials; Spintronics; Superparamagnetism.

1. Introduction

Over recent decades, advances in materials science have highlighted the pivotal role of magnetic materials in successive industrial revolutions, spanning information storage, power electronics and modern biomedical technologies. When material dimensions are reduced to the nanometre scale, magnetic properties no longer follow the conventional laws of bulk magnetism but are instead dominated by quantum, surface and size-confinement effects [1, 2]. The discovery of phenomena such as superparamagnetism, giant magnetoresistance (GMR) and tunnelling magnetoresistance (TMR) opened a new era for spintronics and next-generation data-storage devices [3, 4]. Nevertheless, the rational design and fabrication of magnetic systems with tailored properties require a deep understanding of the complex interplay among chemical composition, crystal structure, microstructure and micromagnetic interactions [5]. Spinel ferrites (e.g., MFe_2O_4), magnetic multilayer thin films and next-generation hard/soft magnetic alloys are currently at the forefront of international research [6]. Beyond their traditional role in electronics, magnetic nanomaterials show considerable promise in biomedicine, particularly for high-contrast magnetic resonance imaging (MRI), bioseparation and magnetic hyperthermia for cancer therapy [7–9].

Between 2020 and 2026, the field of magnetism has undergone several notable transformations: MRAM has become increasingly integrated into mainstream microelectronics, accompanied by a development roadmap for spin–orbit-torque MRAM (SOT-MRAM) [4, 10]; long-range magnetic order has been established in two-dimensional (2D) van der Waals materials [11]; a third elementary magnetic phase, altermagnetism, has been proposed alongside ferromagnetism and antiferromagnetism [12]; and magnetic skyrmions stable at room temperature have been realized in multilayer films [13, 14]. Concurrently, magnetic nanomedicine is shifting from proof-of-concept demonstrations towards standardized measurement protocols and clinical translation [15], while machine learning is accelerating materials discovery at an unprecedented scale [16]. These developments call for an up-to-date review that bridges classical physical principles with emerging research directions.

This review therefore provides a comprehensive and current perspective on magnetic materials, from fundamental theory to pioneering applications. Specifically, it aims to (i) elucidate the physical principles

that govern magnetic behaviour at the nanoscale; (ii) critically compare modern synthesis, fabrication and characterization approaches; (iii) analyse cutting-edge applications in spintronics, skyrmionics, 2D magnetism, biomedicine, environmental science and energy; and (iv) identify the key technical challenges and research directions for the coming decade.

2. Review Methodology

To ensure high methodological rigor, transparency, and reproducibility, this systematic review was conducted in accordance with the Preferred Reporting Items for Systematic Reviews and Meta-Analyses (PRISMA) guidelines, combined with bibliometric analysis. The literature identification, screening, and selection process was executed through four sequential stages:

Stage 1: Comprehensive Literature Search and Identification

Extensive bibliographic searches were performed across three major scientific databases: Scopus, Web of Science (WoS) Core Collection, and PubMed. To cover both fundamental classical theories and the latest research developments up to 2026, the literature search period was defined from 1988 to 2026, with primary weight given to peer-reviewed contributions published between 2020 and 2026. The Boolean search query, applied to the title, abstract and keyword fields, combined material-related terms (e.g., “magnetic nanoparticle*”, “nanomagnet*”, “ferrite*”, “magnetic thin film*”, “multiferroic*”) with phenomenon- and application-related terms (e.g., “superparamagnet*”, “exchange bias”, “spintronic*”, “skyrmion*”, “hyperthermia”, “magnetocaloric”) using the AND/OR operators. The initial automated search yielded a total of 2,850 records.

Stage 2: Duplication Removal and Title/Abstract Screening

In the second stage, 1,120 duplicate records were identified and removed using reference management software. The remaining 1,730 articles underwent title and abstract screening against predefined inclusion and exclusion criteria:

Inclusion criteria: (i) Original research articles and critical state-of-the-art reviews published in high-impact ISI/Scopus-indexed journals; (ii) Studies providing quantitative experimental or theoretical insights into nanomagnetic phenomena, synthesis/fabrication methods, or advanced applications; (iii) English-language peer-reviewed publications.

Exclusion criteria: (i) Conference abstracts, editorials, preprints, non-peer-reviewed reports, and patents; (ii) Studies lacking clear physical mechanisms or experimental validation; (iii) Duplicate reports or articles without full-text access.

After title/abstract screening, 1,490 records were excluded, leaving 240 articles for full-text eligibility assessment.

Stage 3: Full-Text Assessment, Bibliometric Clustering, and Comparative Synthesis

The full texts of the 240 candidate publications were independently evaluated. Bibliometric citation network analysis was applied to group the selected literature into nine key thematic clusters:

(I) Physical fundamentals and surface spin disorder; (II) Spintronics and SOT-MRAM; (III) Synthesis and thin-film fabrication routes; (IV) Magnetic hyperthermia; (V) Dual-mode MRI and targeted drug delivery; (VI) Environmental remediation; (VII) Magnetocaloric cooling; (VIII) Magnetic skyrmions and topological textures; and (IX) 2D van der Waals magnets and altermagnetism.

A critical comparison was then conducted across these clusters, evaluating key figures of merit including specific absorption rate (SAR), tunnelling magnetoresistance (TMR) ratio, spin Hall angle, coercivity (H_c), and critical driving current densities.

Stage 4: Final Sample Inclusion and Reference Verification

Following full-text critical evaluation, **87 representative publications** (encompassing seminal historical works and cutting-edge 2020–2026 breakthroughs) were selected for final synthesis and citation in this review. All bibliographic details (authors, article titles, journal names, volume, page numbers/article IDs, publication years, and DOIs) were verified against publisher records.

[STAGE 1: IDENTIFICATION]
Records identified from Scopus, WoS, and PubMed (n = 2,850)
|
▼
[STAGE 2: SCREENING]
Duplicates removed (n = 1,120) ⟶ Records screened by Title/Abstract (n = 1,730)
|
⊢⟶ Excluded records based on criteria (n = 1,490)
▼
[STAGE 3: ELIGIBILITY]
Full-text articles assessed for eligibility (n = 240)
|
⊢⟶ Excluded after full-text evaluation (n = 153)
▼
[STAGE 4: INCLUSION]
Final representative studies included in systematic review (n = 87)
(Grouped into 9 thematic clusters for critical quantitative comparison)

3. Results and Discussion

3.1. Physical Origins of Magnetic Phenomena at the Nanoscale

3.1.1. Superparamagnetism, the Anisotropy Energy Barrier and the Superparamagnetic Limit

When the size of a ferromagnetic particle is reduced below a critical value D_c (typically from a few to several tens of nanometres, depending on the material and its anisotropy constant), the multidomain configuration gives way to a single-domain state [17, 18]. In this state, all atomic moments are rigidly coupled by exchange and behave collectively as one giant moment, or "macrospin", with $\mu_{tot} \approx 10^3$–$10^5\ \mu_B$ [17–19]. The orientation of this macrospin is governed by the competition between the magnetic anisotropy energy and the thermal energy [17, 18, 20].

Anisotropy energy. For uniaxial anisotropy, $E_A = K_{eff}V \sin^2\theta$, where K_{eff} is the effective anisotropy constant (including magnetocrystalline, shape and surface contributions), V is the particle volume and θ is the angle between the moment and the easy axis [17, 18, 20]. The energy barrier that must be overcome to reverse the magnetization between the two equilibrium orientations is therefore $\Delta E = K_{eff}V$ [17, 18].

Thermal energy. The thermal energy is $E_{th} = k_BT$, where k_B is the Boltzmann constant and T is the absolute temperature [17, 18]. The magnetic relaxation time τ of a single-domain particle follows the Néel–Brown model [18, 21, 22]:

$$\tau = \tau_0 \exp\left(\frac{K_{eff}V}{k_B T}\right) \quad (1)$$

where τ_0 is the attempt time, typically 10^{-9}–10^{-11} s [21, 22]. When the particle becomes so small that $K_{eff}V \ll k_BT$, thermal energy overwhelms the anisotropy barrier and the macrospin flips continuously at a very high rate [17, 18, 23]. If the measurement time of the experimental technique, τ_m (approximately 100 s for DC magnetometry), is much longer than τ, the time-averaged magnetization vanishes, $\langle M \rangle = 0$, in the absence of an applied field [17, 18, 24]. This is the physical origin of superparamagnetism [17, 18, 24]. The thermodynamic boundary separating the blocked state from the superparamagnetic state is defined by the blocking temperature T_B [17, 18, 25]:

$$T_B = \frac{K_{eff}V}{k_B \ln(\tau_m/\tau_0)} \approx \frac{K_{eff}V}{25k_B} \quad (2)$$

The size-driven transition from the multidomain to the single-domain and superparamagnetic states, together with the corresponding evolution of the coercivity and M(H) loops, is illustrated in Figure 1.

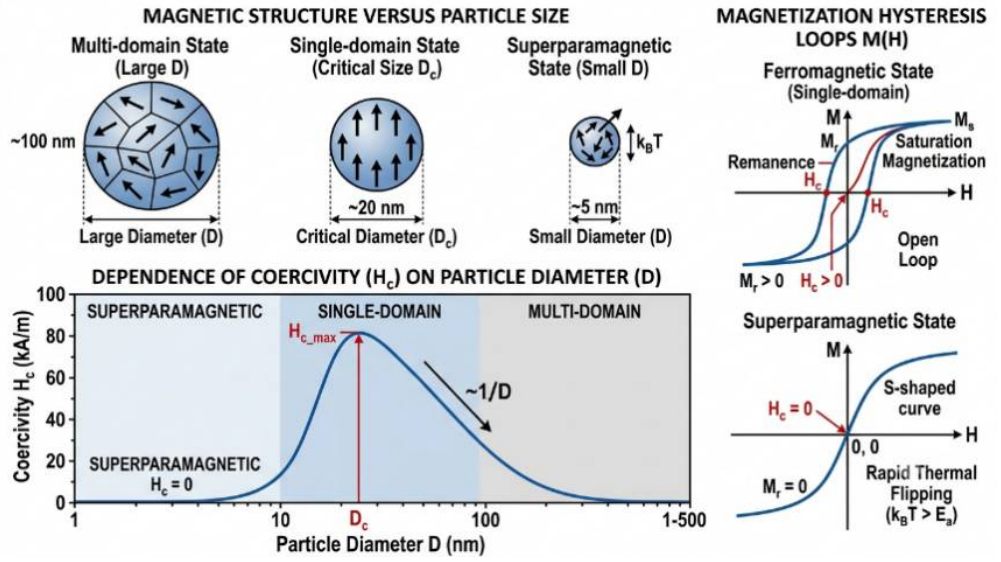


Figure 1. Size-dependent magnetic regimes of nanoparticles: transition from the multidomain to the single-domain and superparamagnetic states, with the corresponding variation of the coercivity H_c and the M(H) hysteresis loops in different temperature ranges.

Equation (2) shows that T_B is extremely sensitive to the particle volume, $V \propto d^3$, where d is the particle diameter [17, 18, 26]. Denoting by D_{sp} ($< D_c$) the threshold diameter for superparamagnetism at the operating temperature, two regimes can be distinguished:

Larger particles ($d > D_{sp}$). The energy barrier $K_{eff}V$ increases steeply, raising T_B above room temperature ($T_B > 300$ K) [17, 18, 27]. The particles retain ferromagnetic (blocked) behaviour with non-zero coercivity ($H_c \neq 0$) and remanence ($M_r \neq 0$) [17, 18, 27].

Smaller particles ($d < D_{sp}$). T_B drops rapidly below the operating temperature [17, 18, 28]. The particles become fully superparamagnetic, with vanishing coercivity ($H_c = 0$) and remanence ($M_r = 0$), which ensures excellent colloidal stability and eliminates agglomeration driven by magnetic attraction [17, 18, 28].

The superparamagnetic limit imposes a fundamental physical barrier on ultrahigh-density magnetic recording: shrinking the grain volume V to increase the areal bit density lowers the barrier $K_{eff}V$ below the thermal-stability criterion ($K_{eff}V \geq 60k_BT$ for long-term data retention), causing random, thermally activated erasure of the stored information [17, 18, 29]. It should be emphasized that the Néel–Brown model was formulated for isolated, non-interacting particles. In real assemblies, dipolar interparticle

interactions modify the distribution of energy barriers, shift T_B and give rise to collective states such as superspin glasses and superferromagnetism [20, 25, 27]. Moreover, a quantitative description of the relaxation time must go beyond the simple Arrhenius law by accounting for the damping parameter and for non-axially symmetric anisotropy [22]. Recent studies have further shown that structural defects and intraparticle spin disorder not only reduce M_s but can also be deliberately exploited to enhance the heating efficiency in magnetic hyperthermia, a strategy termed "design by disorder" [2].

3.1.2. Exchange Bias and Interfacial Exchange Coupling

Exchange bias (EB) is a distinctive micromagnetic phenomenon that arises at the interface between two phases with different magnetic order, most commonly in core/shell architectures that combine a ferromagnetic (FM) phase with an antiferromagnetic (AFM) or ferrimagnetic (FiM) phase [17, 30, 31]. It manifests as a shift of the M(H) hysteresis loop along the field axis, accompanied by a pronounced enhancement of the coercivity H_c [17, 30, 32, 33] (Figure 2). The effect is established when the system is cooled in an applied magnetic field from a temperature above the Néel temperature T_N of the AFM phase to below it, provided that $T_N < T_C$, where T_C is the Curie temperature of the FM phase [30, 32, 34]:

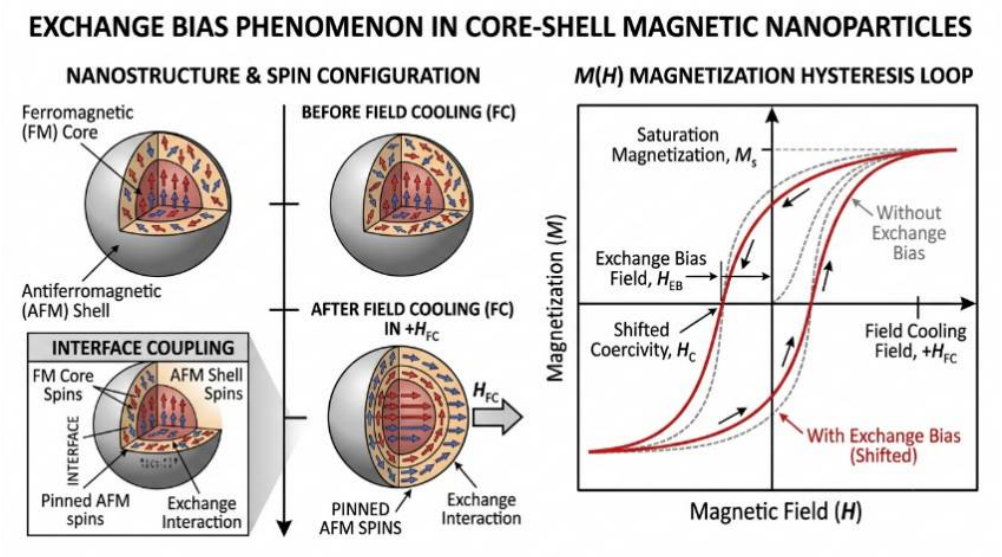


Figure 2. Interfacial spin configuration in FM/AFM core/shell nanoparticles before and after field cooling (FC), and the resulting field-axis shift of the M(H) loop that defines the exchange-bias field H_{EB}.

Interfacial spin alignment. Above T_N, the FM moments follow the external field, whereas the AFM spins are thermally disordered [32, 35]. On cooling below T_N, the AFM spins at the interface become pinned along the direction imposed by the magnetization of the adjacent FM layer [30, 32, 35].

Role of pinned spins. Because the magnetocrystalline anisotropy of the AFM phase is large, the interfacial AFM spins remain pinned even when the external field acting on the FM layer is reversed [30, 32, 35]. This interfacial exchange coupling acts as an internal "bias field" that exerts a torque opposing free reversal of the FM magnetization [32, 35].

The resulting loop shift is quantified by the exchange-bias field H_{EB} [32, 35]:

$$H_{EB} = -\frac{J_{int}}{\mu_0 M_{FM} t_{FM}} \quad (3)$$

where J_{int} is the effective interfacial exchange energy per unit area, μ_0 is the vacuum permeability, and M_{FM} and t_{FM} are the saturation magnetization and the effective thickness of the FM layer, respectively [32, 35]. Engineering FM/AFM or FM/FiM core/shell structures markedly improves thermal stability, introduces additional interfacial anisotropy and allows the superparamagnetic limit to be overcome at

room temperature [17, 32, 36]. The most striking technological implication of EB is precisely this ability to "beat the superparamagnetic limit": ferromagnetic Co nanoparticles embedded in an antiferromagnetic CoO matrix retain a stable magnetization up to temperatures far above those of isolated Co particles, owing to the additional anisotropy generated by interfacial exchange coupling [33]. In nanostructures, the magnitude of H_{EB} depends strongly on interface roughness, shell thickness, the density of uncompensated spins and the field-cooling protocol [34, 35]. At the device level, exchange-pinned layers remain an indispensable component of the spin valves and magnetic tunnel junctions used in hard-disk read heads and MRAM [1, 3].

3.1.3. Magnetic Domain Structure, Domain-Wall Dynamics and Surface Effects

The micromagnetic state of a ferromagnet is determined by the minimization of its total free energy [17, 37, 38]:

$$E_{total} = E_{ex} + E_K + E_D + E_Z + E_\sigma \quad (4)$$

which comprises the exchange, anisotropy, demagnetizing (magnetostatic), Zeeman and magnetoelastic (stress) energies [17, 37, 38]. The formation of domains and domain walls is governed by a critical size D_c [17, 37, 38]:

Multidomain state ($D > D_c$). In bulk material, the demagnetizing energy E_D dominates [37, 38]. To reduce it, the system splits into domains with different magnetization directions separated by Bloch or Néel walls [37, 38]. Magnetization then proceeds via two mechanisms: domain-wall displacement at low fields and moment rotation at high fields [37, 38].

Critical size ($D = D_c$). As the crystal size decreases, the energy cost of forming a domain wall ($E_{DW} \propto r^2$) becomes unfavourable compared with the demagnetizing energy saved ($E_D \propto r^3$) [37, 39]. For $D \leq D_c$, domain walls are no longer energetically sustainable [37, 39]. Following Kittel's energy balance for a sphere, the critical single-domain diameter can be estimated as [37, 38]:

$$D_c = 2R_c \approx \frac{18\gamma_w}{\mu_0 {M_s}^2} = \frac{72\sqrt{AK_{eff}}}{\mu_0 {M_s}^2} \quad (5)$$

where $\gamma_w = 4(AK_{eff})^{1/2}$ is the domain-wall energy per unit area and A is the exchange stiffness. Equation (5) yields D_c of the order of 20 nm for Fe and 80 nm for Fe_3O_4, in line with experimental estimates [38].

Single-domain state ($D \leq D_c$) and surface effects. The particle sustains a single domain with maximal (saturated) magnetization [17, 37]. As the diameter decreases further, the fraction of surface atoms increases sharply, scaling with the surface-to-volume ratio ($S/V \propto 1/d$) [2, 40]. Surface atoms experience broken exchange bonds, which leads to spin canting and a reduction of the saturation magnetization M_s [2, 40]. Two characteristic length scales govern these transitions: the magnetostatic exchange length, $l_{ex} = [2A/(\mu_0 M_s^2)]^{1/2}$, and the domain-wall width, $\delta_w = \pi(A/K)^{1/2}$, where K is the anisotropy constant [38, 39]. For typical 3d ferromagnetic metals, l_{ex} is only a few nanometres; consequently, the reversal mechanism (coherent rotation or curling) is determined by the ratio between the particle size and l_{ex} [39]. In ultrasmall iron oxide particles, a disordered surface-spin shell with a thickness of one to a few unit cells reduces M_s and increases the effective surface anisotropy, a factor that must be considered when designing particles for biomedical applications [2, 40]. Atomistic simulations corroborate these trends: classical Heisenberg-model calculations show that the magnetic characteristics and Curie temperature of Fe nanoparticles depend sensitively on particle size and thermal history [41], whereas Monte Carlo simulations of bulk cobalt reveal the influence of structural configuration, boundary conditions and atomic number on the Curie transition temperature [42]. Similarly, Monte Carlo

simulations of Fe_2O_3 nanocomposite thin films show that the matrix, film size, rotation angle and applied magnetic field shift the Néel transition temperature and the isothermal entropy [43].

As the particle diameter d shrinks well below D_c, the surface-to-volume ratio increases inversely ($S/V \propto 1/d$), placing a substantial fraction of atoms at the surface boundary. These surface atoms inevitably experience broken exchange bonds, reduced coordination numbers, and lattice strain. Consequently, surface spins suffer from severe magnetic disorder and spin canting, a localized departure from parallel alignment. From a micromagnetic standpoint, this introduces a magnetic core-shell architecture within a single particle: a structurally ordered ferromagnetic core exhibiting nominal saturation magnetization (M_s), surrounded by an atomically disordered, spin-canted surface layer. This surface spin disorder drastically reduces the net M_s of sub-10 nm particles while simultaneously generating high surface anisotropy (K_s). Atomistic Heisenberg and Monte Carlo simulations confirm that surface spin canting creates an energy landscape with multiple local minima, leading to open hysteresis loops even above nominal blocking temperatures and shifting the apparent Curie temperature (T_C) as a function of system size and coordination environment [2, 40, 42].

3.2. Advances in Synthesis Methods and Structural Control

3.2.1. Wet-Chemical Routes and Control of Crystal Morphology

Control over the morphology, size and size distribution of magnetic nanoparticles plays a decisive role in determining their micromagnetic properties [17, 44, 45]. The three principal wet-chemical routes are compared schematically in Figure. 3.

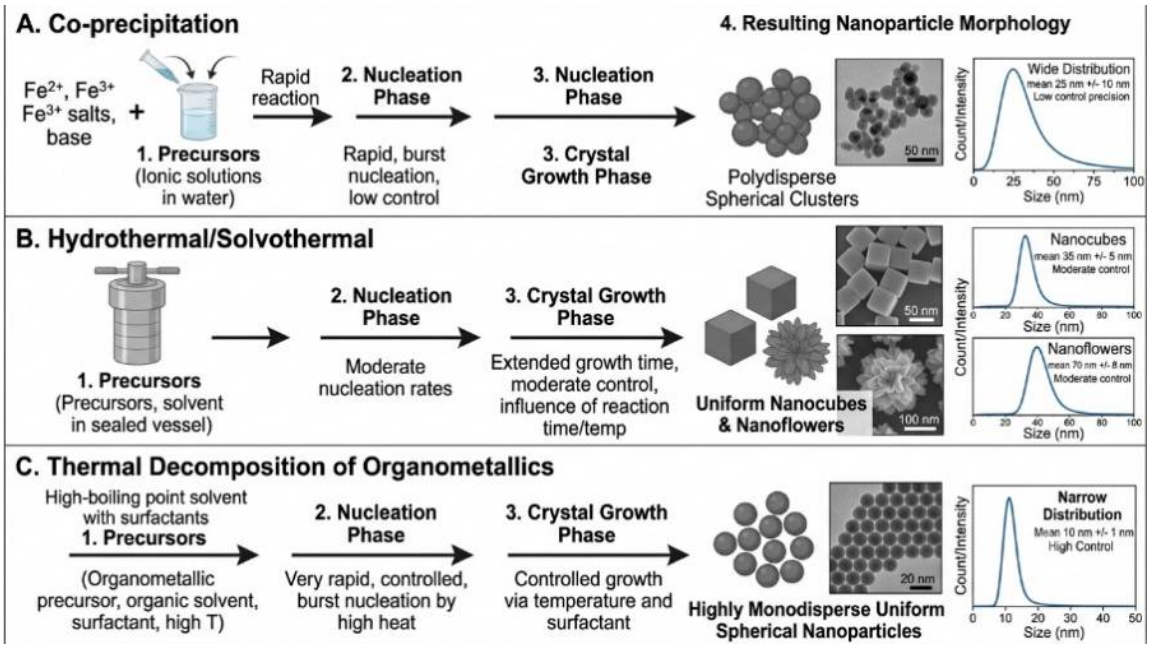


Figure 3. Schematic comparison of the formation mechanisms of magnetic nanoparticles by the three main wet-chemical routes (co-precipitation, hydrothermal/solvothermal synthesis and thermal decomposition of organometallic precursors) and the corresponding degree of control over particle size and crystal morphology.

Co-precipitation. Nanoparticles form through the reaction of metal salts in an alkaline aqueous medium [44, 46]. Although inexpensive and readily scalable, this method usually yields broad size distributions and sub-optimal crystallinity [44, 46].

Hydrothermal/solvothermal synthesis. Reactions are carried out at elevated temperature and pressure in a sealed autoclave [5, 17, 47]. This approach produces highly crystalline particles and enables

good control over the exposed crystal facets (facet engineering) [5, 17, 47].

Thermal decomposition of organometallic precursors. Metal–organic precursors are decomposed in high-boiling solvents (> 300 °C) in the presence of surfactants such as oleic acid or oleylamine [48–50]. This route offers excellent control and produces monodisperse particles with a size standard deviation below 5% [48–50].

Since 2020, a prominent trend has been the shift towards green and continuous synthesis: microwave-assisted polyol and hydrothermal methods, biosynthesis using plant extracts and, in particular, microfluidic flow chemistry, which enables nucleation–growth kinetics to be controlled with high batch-to-batch reproducibility [5]. Standardization of synthesis and characterization protocols (core size, hydrodynamic size, anisotropy distribution and hysteresis losses) is regarded as a prerequisite for inter-laboratory comparability and for the clinical translation of magnetic nanoparticles [8, 15]. The microstructural attributes, magnetic performance and application domains of the main classes of nanomagnetic materials are summarized in Table 1.

Table 1. Comparison of the microstructural attributes, magnetic performance and application domains of the main classes of nanomagnetic materials.

Material class	Typical structure and size	M_s (emu g^{-1})	H_c (Oe)	Key figure of merit	Main advantages	Main limitations	Target applications
Spinel iron oxides (Fe_3O_4, γ-Fe_2O_3)	Spheres; core/shell (5–20 nm)	60–85	0–50 (superpara-magnetic)	SAR: 50–300 W g^{-1} (f = 300 kHz, H = 10 kA m^{-1})	High biosafety; FDA-approved formulations; low-cost synthesis	Moderate M_s; surface oxidation	Magnetic hyperthermia; T_2 MRI contrast; drug delivery
Substituted ferrites / solid solutions ($Mn_{1-x}Zn_xFe_2O_4$, $CoFe_2O_4$)	Cubes; nanoflowers (10–30 nm)	80–110	100–3000	SAR: 500–2500 W g^{-1}	Tunable anisotropy and Curie temperature	Higher toxicity (Co, Ni); complex synthesis	High-efficiency hyperthermia; magnetic sensors
Magnetic metal alloys (FePt, FeCo)	Monodisperse particles; core/shell (3–10 nm)	120–200	1000–15000 (hard magnetic)	$K_u \approx 7 \times 10^6$ J m^{-3} ($L1_0$ FePt)	Very high M_s and K; thermal stability at sizes < 5 nm	Strong oxidation; costly raw materials (Pt)	Ultrahigh-density recording (HAMR); exchange-spring and hard magnets
Spintronic multilayers (CoFeB/MgO/CoFeB)	MTJ stacks; ultrathin films (1–3 nm)	Thickness-dependent	Set by interfacial pinning	TMR: 150–600% (room temperature)	Spin polarization P ≈ 85%; sub-ns switching	Requires atomic-level deposition control	SOT-MRAM; read-head sensors

Material class	Typical structure and size	M_s (emu g^{-1})	H_c (Oe)	Key figure of merit	Main advantages	Main limitations	Target applications
Topological spin textures (magnetic skyrmions)	2D/3D spin whirls (10–100 nm)	Local spin texture	Very low driving current	Driving current density down to ~10^6 A m^{-2} (vs. 10^{11}–10^{12} A m^{-2} for domain walls)	Topological protection; nanoscale size; low-power control	Skyrmion Hall effect; defect pinning; single-skyrmion writing/reading	Racetrack memory; logic gates; neuromorphic/probabilistic computing

Representative values compiled from Refs. [3, 4, 7, 13–15, 17, 28, 29].

A critical comparative analysis of the material classes presented in Table 1 reveals fundamental physical trade-offs between intrinsic magnetic properties, chemical stability, and target applications. Spinel iron oxides (Fe_3O_4, γ-Fe_2O_3) offer superior biocompatibility, low toxicity, and established regulatory approvals, making them the primary choice for clinical nanomedicine. However, their moderate saturation magnetization ($M_s \approx 60$–85 emu·g^{-1}) limits their specific absorption rate (SAR) in magnetic hyperthermia compared to substituted ferrites ($Mn_{1-x}Zn_xFe_2O_4$). Conversely, high-anisotropy metallic alloys like $L1_0$-FePt achieve exceptionally high energy products and thermal stability at sub-5 nm dimensions, yet their clinical adoption is strictly precluded by heavy-metal toxicity and severe susceptibility to oxidation. In spintronic heterostructures, CoFeB/MgO/CoFeB magnetic tunnel junctions dominate commercial MRAM owing to high room-temperature TMR ratios (>200%), but mandate sub-nanometer interface engineering to prevent interdiffusion and degradation of perpendicular magnetic anisotropy.

3.2.2. Physical and Electrochemical Fabrication of Thin Films and Multilayers with Atomic-Scale Control

For spintronic devices and magnetic thin films, control over the interface at the atomic scale is essential [17, 51, 52]. The main deposition techniques are compared in Table 2.

Table 2. Comparative assessment of methods for synthesizing magnetic nanoparticles and fabricating magnetic thin films.

Method	Material system	Size and morphology control	Purity and crystallinity	Industrial scalability	Key advantages	Main drawbacks
Co-precipitation [44, 46]	Oxide nanoparticles; ferrites	Low (PDI > 0.3)	Moderate (post-annealing often needed)	Very high (kilogram scale)	Low cost; simple process; no toxic reagents	Broad size distribution; limited batch-to-batch reproducibility
Hydrothermal / solvothermal [5, 47]	Complex oxides; nanocubes, nanoflowers	Good to very good	High (well-crystallized)	Moderate	Facet engineering; high M_s	High-pressure/high-temperature equipment; long reaction times

Method	Material system	Size and morphology control	Purity and crystallinity	Industrial scalability	Key advantages	Main drawbacks
Thermal decomposition [48–50]	Monodisperse Fe_3O_4, FePt	Excellent (SD < 5%)	Very high	Moderate to low	Excellent monodispersity; nanometre-level size control	Toxic organic solvents; high cost; phase transfer to water required
Magnetron sputtering [54, 55]	Metallic films; MTJs	Ångström-level thickness control	High	Very high (wafer scale)	High uniformity; fast deposition; industry standard	Costly vacuum equipment; unsuitable for free-standing nanoparticles
Atomic layer deposition [56, 57]	Ultrathin oxide films	Self-limiting (one monolayer per cycle)	Very high	High (wafer scale, slow)	Conformal coating of 3D structures; Ångström-level thickness control	Slow growth (~0.1 nm per cycle); limited precursors for magnetic metals
Electrochemical deposition [58–61]	Soft-magnetic Fe–Co–Ni, Ni–Co–Fe and Fe–Ni alloy films on conductive substrates (e.g., ITO)	Good (tuned by bath composition, pH, potential/current and galvanostatic pretreatment)	Moderate to high (nanocrystalline; fcc (111) texture)	High (non-vacuum, room temperature)	Low cost; simple set-up; tunable composition, texture and coercivity	Conductive substrate required; anomalous co-deposition and hydrogen evolution complicate composition control

PDI: polydispersity index; SD: standard deviation of the size distribution.

Pulsed laser deposition (PLD). A short-wavelength pulsed laser ablates a target, generating a plasma plume that condenses on the substrate; the technique preserves the stoichiometry of complex oxides [51, 53].

Magnetron sputtering. This is the industrial standard for metallic magnetic multilayers (FM/NM/FM), offering high thickness uniformity and fast deposition rates [54, 55].

Atomic layer deposition (ALD). Based on self-limiting surface reactions between gaseous precursors, ALD allows thickness to be controlled with monolayer precision [56, 57].

Electrochemical deposition (ED). As a low-cost, non-vacuum and room-temperature alternative, ED enables the growth of nanocrystalline soft-magnetic alloy films on conductive substrates such as indium tin oxide (ITO). In Fe–Co–Ni films, increasing the Co ion concentration in the plating solution raises the Co

content, preserves the anomalous co-deposition behaviour and reduces the crystallite size, thereby tuning the magnetic response [58]. A galvanostatic pretreatment step prior to deposition improves crystal quality and surface morphology and tunes the magnetic characteristics of Ni–Co–Fe/ITO alloys [59]; for Fe_{15}–Ni_{85}/ITO films, it strengthens the (111) texture, decreases the crystallite size and significantly lowers the coercivity [60]. Likewise, the electrolyte pH provides an additional handle on composition, surface roughness, particle size and magnetic properties [61].

Mechanistically, the microstructural texture, crystallite size, and coercive field (H_c) can be systematically tailored by tuning bath chemistry and electrodeposition kinetics. Increasing the Co^{2+} concentration in ternary Fe–Co–Ni plating baths promotes cobalt incorporation while governing anomalous co-deposition, wherein the less noble metals (Fe, Co) deposit preferentially over Ni. Applying a galvanostatic pretreatment pulse prior to film growth alters initial nucleation density, resulting in a stronger (111) crystallographic texture, reduced surface roughness, and refined grain boundaries. In $Fe_{15}Ni_{85}$/ITO alloy films, this structural refinement minimizes domain-wall pinning at grain boundaries, dramatically reducing coercivity H_c and boosting magnetic permeability. Furthermore, modulating the electrolyte pH controls H^+ reduction side-reactions, thereby suppressing hydroxide precipitation and yielding dense, smooth magnetic deposits with enhanced soft-magnetic performance [58–61].

Other routes to magnetic composites and nanostructured alloys. Magnetic functionality can also be imparted to carbon-based and bulk metallic systems. Chemical vapour deposition of carbon nanotube/nanosphere coatings using a Ni–Co–Fe–P catalyst markedly enhances the magnetic properties of carbon fibres [62], while electroless deposition yields GO–CoNiFeP nanocomposites whose structural evolution and thermal stabilization depend on the processing conditions [63]. In bulk alloys, severe plastic deformation by high-pressure torsion produces nanostructured AuCo alloys whose magnetic properties and thermal stability are governed by the deformation-induced microstructure [64]. These top-down and hybrid routes complement wet-chemical and vacuum-deposition methods for applications that require magnetic coatings, electromagnetic functionality or metastable alloy phases.

An emerging fabrication route is the assembly of van der Waals heterostructures from magnetic monolayers (CrI_3, Fe_3GeTe_2, CrSBr, etc.) by exfoliation and deterministic transfer or by molecular-beam epitaxy. The atomically flat interfaces, low intermixing and proximity effects of these heterostructures are expected to enable breakthroughs for MRAM at advanced technology nodes [52]. However, wafer-scale growth and the environmental stability of most 2D magnets remain major obstacles [11].

3.3. Frontier Applications

3.3.1. Spintronics, SOT-MRAM and Brain-Inspired Computing

Spintronics exploits both the charge and the spin of the electron to realize non-volatile, low-dissipation devices with very high operating speeds [17, 65, 66] (Figure. 4).

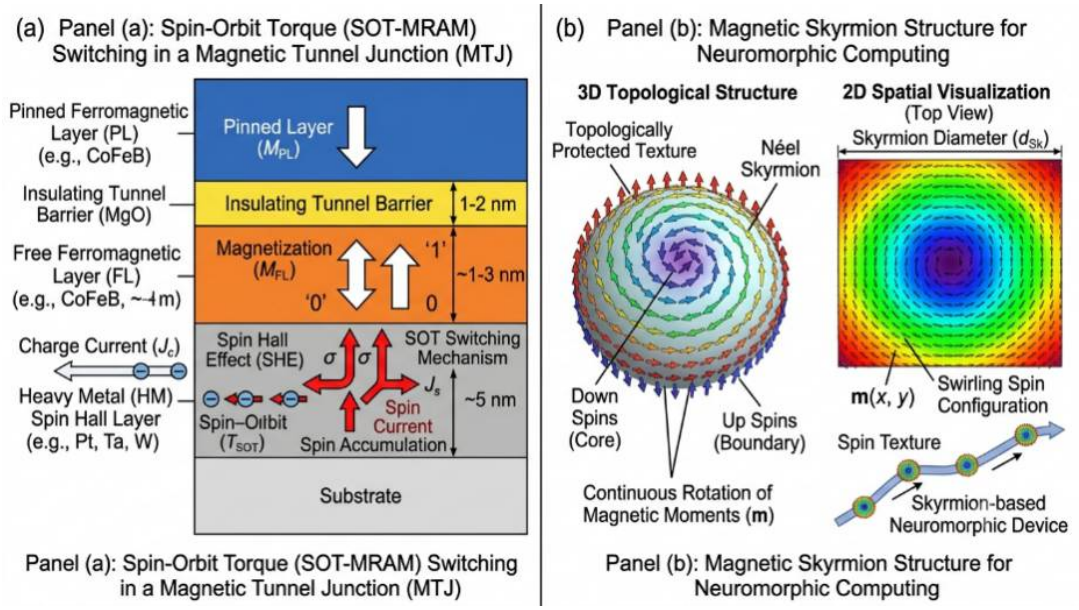


Figure. 4. Nanomagnetic materials in next-generation spintronics: (a) magnetic tunnel junction (MTJ) switched by spin–orbit torque (SOT-MRAM); (b) topologically protected magnetic skyrmion texture for neuromorphic computing.

SOT-MRAM. The spin Hall and Rashba effects in a heavy-metal layer generate a transverse spin current that switches the free-layer magnetization with sub-nanosecond write times (< 1 ns) and virtually unlimited write endurance [10, 65, 67].

Oxide-based TMR devices. Half-metallic oxides with near-100% spin polarization are exploited to maximize the TMR ratio, although sustaining large TMR at room temperature remains challenging [17, 68, 69].

Multiferroic oxide films. Bismuth ferrite ($BiFeO_3$)-based films, in which ferroelectric and magnetic orders coexist at room temperature, offer a route towards electric-field control of magnetism. Zr and Dy co-substitution tunes the optical and multiferroic properties of $BiFeO_3$ thin films [70]; Bi_2O_3/Fe_2O_3 deposits impart multiferroic behaviour to the functionalized surface of flexible substrates [71]; and multiferroic films grown on semiconductor nanotube arrays exhibit resistive switching suitable for non-volatile memory elements [72]. Reducing leakage currents and strengthening the magnetoelectric coupling at room temperature remain the main challenges for device integration.

Neuromorphic computing with domain walls and skyrmions. The motion of domain walls or of topologically protected skyrmions can emulate the plasticity of biological synapses and neurons [68, 73, 74]. Industrially, STT-MRAM has already been integrated as embedded memory in CMOS process lines, whereas SOT-MRAM is regarded as a candidate to replace SRAM in cache memory because its separate read and write paths improve endurance and switching speed [4, 10]. Key challenges include increasing the charge-to-spin conversion efficiency (spin Hall angle), achieving deterministic field-free switching and reducing the footprint of the three-terminal cell [10, 67]. In brain-inspired computing, skyrmion-based artificial synapses whose synaptic weight can be modulated by current pulses have been demonstrated experimentally [73, 75].

3.3.2. Smart Biomedicine, Dual-Mode Imaging and Precision Medicine

The multifunctional use of magnetic nanoparticles in precision medicine is illustrated in Fig. 5, encompassing magnetic hyperthermia for tumour ablation, T1/T2 dual-mode MRI for diagnostic imaging [76], and magnetically guided targeted drug release.

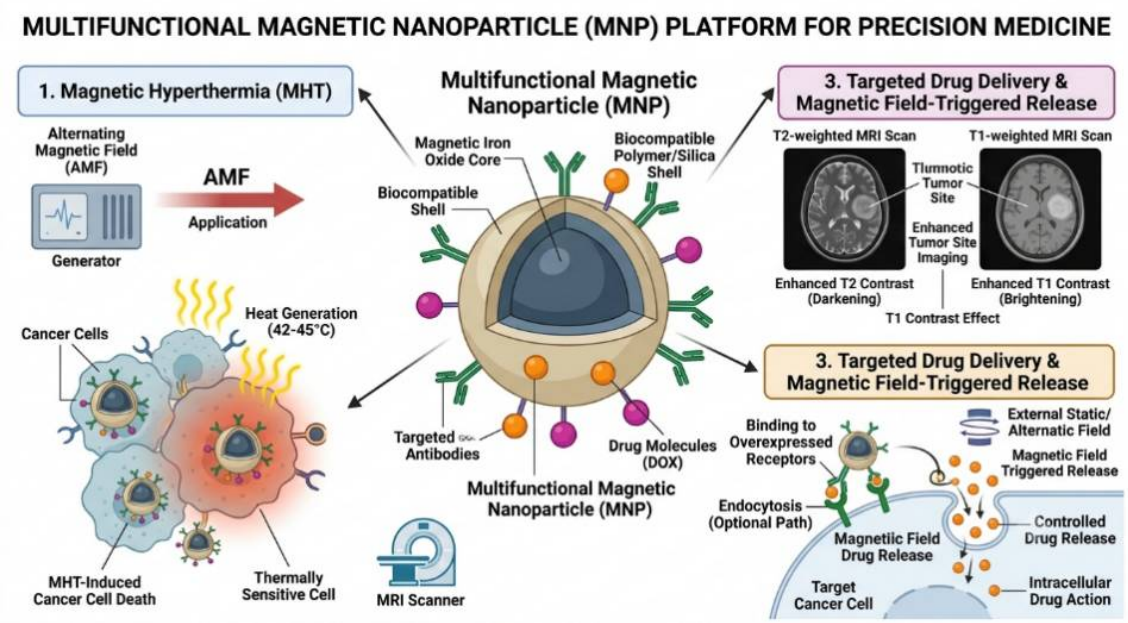


Fig. 5. Multifunctional magnetic nanoparticles for precision medicine: magnetic hyperthermia for tumour ablation, T_1/T_2 dual-mode MRI and magnetically guided targeted drug release.

Magnetic hyperthermia. Under an alternating magnetic field (f ≈ 100–400 kHz), nanoparticles absorb field energy and release heat through Néel and Brown relaxation losses [17, 77]. The intratumoural temperature is maintained at about 42–45 °C to destroy cancer cells while sparing healthy tissue [17, 77]. The heating efficiency is quantified by the specific absorption rate (SAR) or the intrinsic loss power (ILP) and depends strongly on particle size, morphology, anisotropy, aggregation state and field conditions; for physiological safety, the product H·f is usually kept below about 5×10^9 A m^{-1} s^{-1} [7, 17]. Recent studies focus on nanoclusters, cubic and flower-shaped particles and combination therapies (thermo-chemotherapy and magneto-photothermal therapy), together with standardized calorimetric measurements and the integration of magnetic particle imaging (MPI) for in situ quantification of the thermal dose [7, 15].

Dual-mode T_1/T_2 MRI contrast agents. Combining a bright T_1 contrast component (e.g., Gd^{3+} or ultrasmall Fe_3O_4) and a dark T_2 component within a single nanoparticle helps eliminate false-positive signals in diagnostic imaging [9, 78, 79]. In view of concerns about gadolinium retention in the body, ultrasmall iron oxide nanoparticles (diameter below about 5 nm) with low r_2/r_1 ratios are being developed as alternative T_1 agents with better biocompatibility and biodegradability [9, 79, 80].

Targeted drug delivery. Nanoparticle surfaces are functionalized with biomolecules (antibodies, aptamers) and guided by an external magnetic field to release chemotherapeutic drugs precisely at the target tissue [17, 78, 81]. Beyond hyperthermia, superparamagnetic iron oxide nanoparticles (SPIONs) are exploited for magneto-mechanical therapy under low-frequency fields, for the generation of reactive oxygen species (ROS) and for modulating macrophage polarization in cancer immunotherapy [8]. However, the potential toxicity of magnetic nanoparticles, which is related to their large surface area, chemical composition, size, dose, organ accumulation and degradation and clearance pathways, must be assessed systematically [82].

3.3.3. Environmental Remediation and Green Energy Conversion

Magnetically recoverable photocatalysts. Integrating magnetic nanostructures with semiconductor photocatalysts (e.g., TiO_2, ZnO) yields hybrid materials that degrade toxic organic

pollutants and can be rapidly recovered with a magnetic field [6, 83]. Spinel ferrites MFe_2O_4 (M = Co, Cu, Mn, Ni, Zn) have emerged as heterogeneous catalysts for Fenton and photo-Fenton reactions owing to their low cost, narrow band gap, chemical stability and magnetic recoverability; their catalytic activity depends on the nature of the M cation, the synthesis method, the annealing temperature and operating conditions (pH, H_2O_2 concentration and light source) [6]. Magnetically recoverable nanocatalysts simultaneously solve the problems of phase separation and catalyst reuse [83].

Magnetocaloric materials. The magnetic entropy change (ΔS_M) induced when a material is placed in an external field can be harnessed for high-efficiency, environmentally friendly refrigeration that avoids greenhouse-gas refrigerants [84–87]. Magnetocaloric energy conversion extends beyond refrigeration to heat pumping, the liquefaction of hydrogen and other gases and the conversion of low-grade waste heat into useful work [87]. The main current obstacles are the thermal and magnetic hysteresis of first-order phase-transition materials, the cost of the rare-earth permanent magnets used to generate the field and the heat-transfer efficiency of the regenerator [85, 87]. Atomistic Monte Carlo simulations offer a complementary route for predicting how the film size, matrix and applied field shape the isothermal entropy near magnetic phase transitions [43].

3.3.4. Magnetic Skyrmions, 2D van der Waals Magnets and Altermagnets

Magnetic skyrmions are topologically protected, vortex-like spin textures stabilized by the Dzyaloshinskii–Moriya interaction (DMI) in non-centrosymmetric crystals or at heavy-metal/ferromagnet interfaces [13, 74]. Their small size (from a few to several hundred nanometres), the low current densities required to drive them and their stability at room temperature in multilayer films make skyrmions promising candidates for racetrack memories, logic gates and probabilistic computing [14, 68]. Current challenges include the skyrmion Hall effect, which deflects their trajectories, pinning by defects and the reliable nucleation and detection of individual skyrmions [13, 14]. 2D van der Waals magnets allow magnetic order to be controlled by electric fields, strain and twisted stacking, with potential applications in topological magnonics, low-power spintronics, quantum computing and optical communications [11]. In parallel, altermagnets, a magnetic phase with zero net magnetization like antiferromagnets but with spin-split electronic bands like ferromagnets, promise to combine terahertz dynamics, immunity to stray fields and strongly spin-polarized currents for a new generation of spintronic devices [12].

3.4. Open Challenges and Future Research Directions

Despite the substantial progress achieved in nanomagnetic materials and their technological integration, several critical bottlenecks continue to impede their full-scale transition from laboratory demonstrations to commercial and clinical deployment. Addressing these fundamental and practical hurdles requires concerted interdisciplinary research spanning physics, materials science, bioengineering, and data science.

3.4.1. Microstructural Reproducibility and Standardized Protocols

A persistent challenge in the field of synthetic nanomagnetism is the high sensitivity of functional parameters—such as specific absorption rate (SAR), transverse (r_2) and longitudinal (r_1) relaxivities, coercive field (H_c), and switching current thresholds (J_c)—to subtle variations in physical dimensions, surface stoichiometry, and aggregation state [5, 15]. Inter-laboratory discrepancies frequently arise due to the lack of standardized measurement protocols, particularly regarding applied field frequency, amplitude, and thermal isolation during calorimetric characterization [15]. To establish reliable quantitative benchmarks, standardized operating procedures (SOPs) and reference materials must be

universally adopted for evaluating core size, hydrodynamic volume, surface spin disorder, and magnetic hysteresis losses [8, 15].

3.4.2. Biosafety, Long-Term Fate, and Clinical Translation

While superparamagnetic iron oxide nanoparticles (SPIONs) have gained FDA approval for specific clinical indications, the broader biomedical application of multifunctional magnetic nanostructures remains constrained by concerns over long-term biosafety [8, 82]. The high surface-to-volume ratio (S/V) of sub-10 nm particles enhances surface reactivity and spin disorder, but also escalates potential cytotoxicity via reactive oxygen species (ROS) generation and intracellular degradation pathways [2, 82]. The in vivo degradation kinetics, organ bioaccumulation (particularly in the liver and spleen), immune cell interaction, and clearance dynamics of elements beyond iron (e.g., Co, Ni, Mn, rare-earth dopants) must be systematically quantified under physiological conditions prior to broad clinical adoption [7, 82].

3.4.3. Critical Raw Materials and Rare-Earth Substitution

The heavy reliance on critical and strategic elements—such as Nd and Dy for high-energy permanent magnets, and Pt and Ir for spintronic multilayers and heavy-metal spin-orbit torque (SOT) channels—presents severe economic and supply-chain vulnerabilities [1, 4, 85]. Consequently, a major research directive focuses on developing rare-earth-free or rare-earth-lean hard magnetic materials [1, 85]. Strategies such as self-assembled exchange-spring nanocomposites (coupling a hard magnetic core with a soft magnetic matrix) and metastable phases ($L1_0$-FeNi) offer potential pathways to achieve elevated energy products (BH_{max}) while eliminating critical metal dependence [36, 85].

3.4.4. Scalability, Interface Quality, and CMOS Integration

Translating cutting-edge quantum magnetic phenomena—such as room-temperature skyrmions, two-dimensional (2D) van der Waals magnets, and altermagnetic spin splitting—into scalable microelectronic platforms faces severe manufacturing constraints [4, 11, 12, 14]. Achieving atomic-scale interface sharpness, suppressing atomic interdiffusion, and maintaining perpendicular magnetic anisotropy (PMA) across full 300 mm wafer configurations remain critical engineering goals [4, 52, 54]. Furthermore, fabricating spin-torque devices requires strict thermal budget compatibility with standard back-end-of-line (BEOL) CMOS processing, alongside low driving current densities ($J_c < 10^6$ A·cm^{-2}) to ensure non-volatile memory endurance and ultra-low power consumption [4, 10, 67].

3.4.5. Machine Learning and Data-Driven Discovery: Opportunities and Limitations

Data-driven material discovery and machine learning (ML) architectures are rapidly transforming magnetism research [16]. Integrating physics-informed neural networks (PINNs) with high-throughput density functional theory (DFT), micromagnetic solvers, and atomistic Heisenberg/Monte Carlo simulations enables high-efficiency screening of chemical compositions, crystal structures, Curie temperatures (T_C), and spin Hall angles (θ_{SH}) [16, 41, 42].

However, the application of ML to nanomagnetic systems is currently subject to three major limitations:

Data Scarcity and Heterogeneity: Experimental datasets reported in the literature often suffer from inconsistent reporting of synthesis conditions, surface capping, and structural defects, leading to noisy training inputs [5, 15, 16].

Microstructural Complexity: Standard ML descriptors encounter difficulties in capturing non-equilibrium, nanoscale phenomena such as surface spin canting, interparticle dipolar coupling, and domain-wall pinning dynamics [2, 20, 37].

Extrapolation Bounds: Machine learning models trained on conventional ferromagnetic or ferrimagnetic phases frequently demonstrate limited predictive power when extrapolated to novel spin topologies, including skyrmion lattices and altermagnetic band structures [12, 13, 16].

Bridging physics-based micromagnetic simulation frameworks with robust experimental data repositories will be essential to realize the full potential of AI-assisted nanomaterial optimization [16].

4. Conclusions

This review systematizes recent progress in nanomagnetic and advanced magnetic materials, spanning microstructural physics, fabrication strategies, and frontier applications. Simultaneous atomic-scale control over size, morphology, anisotropy, and interfaces is essential for tailoring magnetic properties on demand: the energy barrier ($K_{eff}V$) governs the superparamagnetic limit and thermal stability, interfacial exchange coupling helps overcome this threshold, and characteristic lengths (l_{ex} and δ_w) dictate magnetization-reversal mechanisms. Complementary to vacuum deposition, low-cost electrochemical routes effectively tune the texture, crystallite size, and coercivity of soft-magnetic films. These advances drive low-power spintronics and neuromorphic computing (via SOT-MRAM, skyrmions, and 2D van der Waals magnets), precision biomedicine (hyperthermia, MRI, and drug delivery using superparamagnetic iron oxide nanoparticles), environmental remediation, and magnetocaloric energy conversion. Overcoming remaining bottlenecks—including reproducibility, standardized metrology, biosafety, rare-earth reliance, and CMOS integration—through green continuous synthesis, machine-learning-assisted design, and interdisciplinary collaboration will accelerate the translation of nanomagnetic technologies from laboratory to commercialization over the next decade.

Funding: The authors declare that no funds, grants, or other support were received during the preparation of this manuscript.

Data Availability Statement: The data that support the findings of this study are available from the corresponding authors upon reasonable request.

Declaration of competing interest: The authors declare that they have no known competing financial interest or personal relationships that could have appeared to influence the work reported in this paper.

References

[1] E. Y. Vedmedenko, R. K. Kawakami, D. D. Sheka, P. Gambardella, A. Kirilyuk, A. Hirohata, et al., The 2020 magnetism roadmap, J. Phys. D: Appl. Phys. 53, 453001 (2020). https://doi.org/10.1088/1361-6463/ab9d98

[2] A. Lak, S. Disch, P. Bender, Embracing defects and disorder in magnetic nanoparticles, Adv. Sci. 8, 2002682 (2021). https://doi.org/10.1002/advs.202002682

[3] A. Hirohata, K. Yamada, Y. Nakatani, I.-L. Prejbeanu, B. Diény, P. Pirro, B. Hillebrands, Review on spintronics: Principles and device applications, J. Magn. Magn. Mater. 509, 166711 (2020). https://doi.org/10.1016/j.jmmm.2020.166711

[4] B. Dieny, I. L. Prejbeanu, K. Garello, P. Gambardella, P. Freitas, R. Lehndorff, et al., Opportunities and challenges for spintronics in the microelectronics industry, Nat. Electron. 3, 446–459 (2020). https://doi.org/10.1038/s41928-020-0461-5

[5] A. Ali, T. Shah, R. Ullah, P. Zhou, M. Guo, M. Ovais, Z. Tan, Y. Rui, Review on recent progress in

magnetic nanoparticles: Synthesis, characterization, and diverse applications, Front. Chem. 9, 629054 (2021). https://doi.org/10.3389/fchem.2021.629054

[6] A. Soufi, H. Hajjaoui, R. Elmoubarki, M. Abdennouri, S. Qourzal, N. Barka, Spinel ferrites nanoparticles: Synthesis methods and application in heterogeneous Fenton oxidation of organic pollutants – A review, Appl. Surf. Sci. Adv. 6, 100145 (2021). https://doi.org/10.1016/j.apsadv.2021.100145

[7] H. Gavilán, S. K. Avugadda, T. Fernández-Cabada, N. Soni, M. Cassani, B. T. Mai, R. Chantrell, T. Pellegrino, Magnetic nanoparticles and clusters for magnetic hyperthermia: optimizing their heat performance and developing combinatorial therapies to tackle cancer, Chem. Soc. Rev. 50, 11614–11667 (2021). https://doi.org/10.1039/D1CS00427A

[8] T. Vangijzegem, V. Lecomte, I. Ternad, L. Van Leuven, R. N. Muller, D. Stanicki, S. Laurent, Superparamagnetic iron oxide nanoparticles (SPION): From fundamentals to state-of-the-art innovative applications for cancer therapy, Pharmaceutics 15, 236 (2023). https://doi.org/10.3390/pharmaceutics15010236

[9] M. Jeon, M. V. Halbert, Z. R. Stephen, M. Zhang, Iron oxide nanoparticles as T_1 contrast agents for magnetic resonance imaging: Fundamentals, challenges, applications, and prospectives, Adv. Mater. 33, 1906539 (2021). https://doi.org/10.1002/adma.201906539

[10] Q. Shao, P. Li, L. Liu, H. Yang, S. Fukami, A. Razavi, et al., Roadmap of spin–orbit torques, IEEE Trans. Magn. 57, 800439 (2021). https://doi.org/10.1109/TMAG.2021.3078583

[11] Q. H. Wang, A. Bedoya-Pinto, M. Blei, A. H. Dismukes, A. Hamo, S. Jenkins, et al., The magnetic genome of two-dimensional van der Waals materials, ACS Nano 16, 6960–7079 (2022). https://doi.org/10.1021/acsnano.1c09150

[12] L. Šmejkal, J. Sinova, T. Jungwirth, Emerging research landscape of altermagnetism, Phys. Rev. X 12, 040501 (2022). https://doi.org/10.1103/PhysRevX.12.040501

[13] Y. Tokura, N. Kanazawa, Magnetic skyrmion materials, Chem. Rev. 121, 2857–2897 (2021). https://doi.org/10.1021/acs.chemrev.0c00297

[14] C. Back, V. Cros, H. Ebert, K. Everschor-Sitte, A. Fert, M. Garst, et al., The 2020 skyrmionics roadmap, J. Phys. D: Appl. Phys. 53, 363001 (2020). https://doi.org/10.1088/1361-6463/ab8418

[15] I. Rubia-Rodríguez, A. Santana-Otero, S. Spassov, E. Tombácz, C. Johansson, P. De La Presa, et al., Whither magnetic hyperthermia? A tentative roadmap, Materials 14, 706 (2021). https://doi.org/10.3390/ma14040706

[16] A. Merchant, S. Batzner, S. S. Schoenholz, M. Aykol, G. Cheon, E. D. Cubuk, Scaling deep learning for materials discovery, Nature 624, 80–85 (2023). https://doi.org/10.1038/s41586-023-06735-9

[17] E. A. Périgo, G. Hemery, O. Sandre, D. Ortega, E. Garaio, F. Plazaola, F. J. Teran, Fundamentals and advances in magnetic hyperthermia, Appl. Phys. Rev. 2, 041302 (2015). https://doi.org/10.1063/1.4935688

[18] C. P. Bean, J. D. Livingston, Superparamagnetism, J. Appl. Phys. 30, S120–S129 (1959). https://doi.org/10.1063/1.2185850

[19] M. Jamet, W. Wernsdorfer, C. Thirion, D. Mailly, V. Dupuis, P. Mélinon, A. Pérez, Magnetic anisotropy of a single cobalt nanocluster, Phys. Rev. Lett. 86, 4676–4679 (2001). https://doi.org/10.1103/PhysRevLett.86.4676

[20] S. Mørup, E. Tronc, Superparamagnetic relaxation of weakly interacting particles, Phys. Rev. Lett. 72,

3278–3281 (1994). https://doi.org/10.1103/PhysRevLett.72.3278

[21] W. F. Brown Jr., Thermal fluctuations of a single-domain particle, Phys. Rev. 130, 1677–1686 (1963). https://doi.org/10.1103/PhysRev.130.1677

[22] W. T. Coffey, Y. P. Kalmykov, Thermal fluctuations of magnetic nanoparticles: Fifty years after Brown, J. Appl. Phys. 112, 121301 (2012). https://doi.org/10.1063/1.4754272

[23] R. W. Chantrell, J. Popplewell, S. W. Charles, Measurements of particle size distribution parameters in ferrofluids, IEEE Trans. Magn. 14, 975–977 (1978). https://doi.org/10.1109/TMAG.1978.1059918

[24] A.-H. Lu, E. L. Salabas, F. Schüth, Magnetic nanoparticles: Synthesis, protection, functionalization, and application, Angew. Chem. Int. Ed. 46, 1222–1244 (2007). https://doi.org/10.1002/anie.200602866

[25] J. L. Dormann, D. Fiorani, E. Tronc, Magnetic relaxation in fine-particle systems, Adv. Chem. Phys. 98, 283–494 (1997). https://doi.org/10.1002/9780470141571.ch4

[26] D. L. Leslie-Pelecky, R. D. Rieke, Magnetic properties of nanostructured materials, Chem. Mater. 8, 1770–1783 (1996). https://doi.org/10.1021/cm960077f

[27] S. Bedanta, W. Kleemann, Supermagnetism, J. Phys. D: Appl. Phys. 42, 013001 (2009). https://doi.org/10.1088/0022-3727/42/1/013001

[28] Q. A. Pankhurst, J. Connolly, S. K. Jones, J. Dobson, Applications of magnetic nanoparticles in biomedicine, J. Phys. D: Appl. Phys. 36, R167–R181 (2003). https://doi.org/10.1088/0022-3727/36/13/201

[29] D. Weller, A. Moser, Thermal effect limits in ultrahigh-density magnetic recording, IEEE Trans. Magn. 35, 4423–4439 (1999). https://doi.org/10.1109/20.809134

[30] W. H. Meiklejohn, C. P. Bean, New magnetic anisotropy, Phys. Rev. 102, 1413–1414 (1956). https://doi.org/10.1103/PhysRev.102.1413

[31] A. E. Berkowitz, K. Takano, Exchange anisotropy — a review, J. Magn. Magn. Mater. 200, 552–570 (1999). https://doi.org/10.1016/S0304-8853(99)00453-9

[32] J. Nogués, I. K. Schuller, Exchange bias, J. Magn. Magn. Mater. 192, 203–232 (1999). https://doi.org/10.1016/S0304-8853(98)00266-2

[33] V. Skumryev, S. Stoyanov, Y. Zhang, G. Hadjipanayis, D. Givord, J. Nogués, Beating the superparamagnetic limit with exchange bias, Nature 423, 850–853 (2003). https://doi.org/10.1038/nature01687

[34] S. Giri, M. Patra, S. Majumdar, Exchange bias effect in alloys and compounds, J. Phys.: Condens. Matter 23, 073201 (2011). https://doi.org/10.1088/0953-8984/23/7/073201

[35] J. Nogués, J. Sort, V. Langlais, V. Skumryev, S. Suriñach, J. S. Muñoz, M. D. Baró, Exchange bias in nanostructures, Phys. Rep. 422, 65–117 (2005). https://doi.org/10.1016/j.physrep.2005.08.004

[36] H. Zeng, J. Li, J. P. Liu, Z. L. Wang, S. Sun, Exchange-coupled nanocomposite magnets by nanoparticle self-assembly, Nature 420, 395–398 (2002). https://doi.org/10.1038/nature01208

[37] C. Kittel, Physical theory of ferromagnetic domains, Rev. Mod. Phys. 21, 541–583 (1949). https://doi.org/10.1103/RevModPhys.21.541

[38] J. M. D. Coey, Magnetism and Magnetic Materials, Cambridge University Press, Cambridge (2010). https://doi.org/10.1017/CBO9780511845000

[39] G. S. Abo, Y.-K. Hong, J. Park, J. Lee, W. Lee, B.-C. Choi, Definition of magnetic exchange length, IEEE Trans. Magn. 49, 4937–4939 (2013). https://doi.org/10.1109/TMAG.2013.2258028

[40] R. H. Kodama, Magnetic nanoparticles, J. Magn. Magn. Mater. 200, 359–372 (1999). https://doi.org/10.1016/S0304-8853(99)00347-9

[41] T. D. Nguyen, C. C. Nguyen, T. T. Nguyen, K. H. Pham, Factors on the magnetic properties of the iron nanoparticles by classical Heisenberg model, Physica B 532, 144–148 (2018). https://doi.org/10.1016/j.physb.2017.08.083

[42] D. Nguyen Trong, T. Tran Quoc, Ş. Ţălu, Influence of structural configurations, boundary conditions, and atomic number on the Curie transition temperature of bulk cobalt: A Monte Carlo simulation study, Nano 20, 2550012 (2025). https://doi.org/10.1142/S1793292025500122

[43] D. Nguyen Trong, V. Cao Long, Ş. Ţălu, The study of the influence of matrix, size, rotation angle, and magnetic field on the isothermal entropy, and the Néel phase transition temperature of Fe_2O_3 nanocomposite thin films by the Monte-Carlo simulation method, Coatings 11, 1209 (2021). https://doi.org/10.3390/coatings11101209

[44] A. K. Gupta, M. Gupta, Synthesis and surface engineering of iron oxide nanoparticles for biomedical applications, Biomaterials 26, 3995–4021 (2005). https://doi.org/10.1016/j.biomaterials.2004.10.012

[45] Y.-w. Jun, J.-w. Seo, J. Cheon, Nanoscaling laws of magnetic nanoparticles and their applicabilities in biomedical sciences, Acc. Chem. Res. 41, 179–189 (2008). https://doi.org/10.1021/ar700121f

[46] S. Laurent, D. Forge, M. Port, A. Roch, C. Robic, L. Vander Elst, R. N. Muller, Magnetic iron oxide nanoparticles: Synthesis, stabilization, vectorization, physicochemical characterizations, and biological applications, Chem. Rev. 108, 2064–2110 (2008). https://doi.org/10.1021/cr068445e

[47] X. Wang, J. Zhuang, Q. Peng, Y. Li, A general strategy for nanocrystal synthesis, Nature 437, 121–124 (2005). https://doi.org/10.1038/nature03968

[48] J. Park, K. An, Y. Hwang, J.-G. Park, H.-J. Noh, J.-Y. Kim, J.-H. Park, N.-M. Hwang, T. Hyeon, Ultra-large-scale syntheses of monodisperse nanocrystals, Nat. Mater. 3, 891–895 (2004). https://doi.org/10.1038/nmat1251

[49] S. Sun, H. Zeng, D. B. Robinson, S. Raoux, P. M. Rice, S. X. Wang, G. Li, Monodisperse MFe_2O_4 (M = Fe, Co, Mn) nanoparticles, J. Am. Chem. Soc. 126, 273–279 (2004). https://doi.org/10.1021/ja0380852

[50] T. Hyeon, Chemical synthesis of magnetic nanoparticles, Chem. Commun. (8), 927–934 (2003). https://doi.org/10.1039/B207789B

[51] D. H. Lowndes, D. B. Geohegan, A. A. Puretzky, D. P. Norton, C. M. Rouleau, Synthesis of novel thin-film materials by pulsed laser deposition, Science 273, 898–903 (1996). https://doi.org/10.1126/science.273.5277.898

[52] H. Yang, S. O. Valenzuela, M. Chshiev, S. Couet, B. Dieny, B. Dlubak, et al., Two-dimensional materials prospects for non-volatile spintronic memories, Nature 606, 663–673 (2022). https://doi.org/10.1038/s41586-022-04768-0

[53] H. Y. Hwang, Y. Iwasa, M. Kawasaki, B. Keimer, N. Nagaosa, Y. Tokura, Emergent phenomena at oxide interfaces, Nat. Mater. 11, 103–113 (2012). https://doi.org/10.1038/nmat3223

[54] S. Yuasa, T. Nagahama, A. Fukushima, Y. Suzuki, K. Ando, Giant room-temperature magnetoresistance in single-crystal Fe/MgO/Fe magnetic tunnel junctions, Nat. Mater. 3, 868–871 (2004). https://doi.org/10.1038/nmat1257

[55] S. S. P. Parkin, C. Kaiser, A. Panchula, P. M. Rice, B. Hughes, M. Samant, S.-H. Yang, Giant tunnelling magnetoresistance at room temperature with MgO (100) tunnel barriers, Nat. Mater. 3, 862–867 (2004). https://doi.org/10.1038/nmat1256

[56] S. M. George, Atomic layer deposition: An overview, Chem. Rev. 110, 111–131 (2010). https://doi.org/10.1021/cr900056b

[57] M. Knez, K. Nielsch, L. Niinistö, Synthesis and surface engineering of complex nanostructures by atomic layer deposition, Adv. Mater. 19, 3425–3438 (2007). https://doi.org/10.1002/adma.200700079

[58] V. Cao Long, U. Saraç, M. C. Baykul, L. Duong Trong, Ş. Ţălu, D. Nguyen Trong, Electrochemical deposition of Fe–Co–Ni samples with different Co contents and characterization of their microstructural and magnetic properties, Coatings 12, 346 (2022). https://doi.org/10.3390/coatings12030346

[59] U. Saraç, D. Nguyen Trong, M. C. Baykul, V. Cao Long, Ş. Ţălu, Tuning structural properties, morphology and magnetic characteristics of nanostructured Ni–Co–Fe/ITO ternary alloys by galvanostatic pretreatment process, Microsc. Res. Tech. 85, 3945–3954 (2022). https://doi.org/10.1002/jemt.24235

[60] U. Saraç, M. C. Baykul, G. Dındış, D. Nguyen Trong, K. Malik, P. L. Doan, V. Cao Long, Ş. Ţălu, Improvement of some physical and magnetic properties of nanocrystalline Fe_{15}–Ni_{85}/ITO thin films by galvanostatic pretreatment process, Mater. Today Commun. 35, 106067 (2023). https://doi.org/10.1016/j.mtcomm.2023.106067

[61] U. Saraç, D. Nguyen Trong, M. C. Baykul, V. Cao Long, P. Nguyen Dang, D. Phuong Lan, Ş. Ţălu, Electrolyte pH dependence of composition, roughness parameters, particle diameter and magnetic features of nanostructured Fe–Co–Ni/ITO deposits prepared by electrochemical deposition method, J. Microsc. 290, 106–116 (2023). https://doi.org/10.1111/jmi.13180

[62] N. Patra, Ş. Ţălu, Enhanced magnetic properties of carbon fibers through carbon nanotube/nanosphere coating with Ni–Co–Fe–P catalyst via chemical vapor deposition, Diamond Relat. Mater. 157, 112527 (2025). https://doi.org/10.1016/j.diamond.2025.112527

[63] P. Ramesh, N. S. M. P. Latha Devi, Ş. Ţălu, N. Patra, Structural evolution and thermal stabilization of GO–CoNiFeP nanocomposites prepared by electroless deposition, J. Mater. Sci.: Mater. Eng. 21, 153 (2026). https://doi.org/10.1186/s40712-026-00580-0

[64] T. P. Tolmachev, I. A. Morozov, S. A. Petrova, D. A. Shishkin, E. A. Tolmacheva, V. P. Pilyugin, Ş. Ţălu, Magnetic properties and thermal stability of AuCo alloy obtained by high-pressure torsion, Metals 15, 118 (2025). https://doi.org/10.3390/met15020118

[65] L. Liu, C.-F. Pai, Y. Li, H. W. Tseng, D. C. Ralph, R. A. Buhrman, Spin-torque switching with the giant spin Hall effect of tantalum, Science 336, 555–558 (2012). https://doi.org/10.1126/science.1218197

[66] I. Žutić, J. Fabian, S. Das Sarma, Spintronics: Fundamentals and applications, Rev. Mod. Phys. 76, 323–410 (2004). https://doi.org/10.1103/RevModPhys.76.323

[67] A. Manchon, J. Železný, I. M. Miron, T. Jungwirth, J. Sinova, A. Thiaville, K. Garello, P. Gambardella, Current-induced spin-orbit torques in ferromagnetic and antiferromagnetic systems, Rev. Mod. Phys. 91, 035004 (2019). https://doi.org/10.1103/RevModPhys.91.035004

[68] A. Fert, V. Cros, J. Sampaio, Skyrmions on the track, Nat. Nanotechnol. 8, 152–156 (2013). https://doi.org/10.1038/nnano.2013.29

[69] M. Bibes, A. Barthélémy, Oxide spintronics, IEEE Trans. Electron Devices 54, 1003–1023 (2007). https://doi.org/10.1109/TED.2007.894366

[70] A. Sathiya Priya, D. Geetha, J. M. Siqueiros, Ş. Ţălu, Tunable optical and multiferroic properties of zirconium and dysprosium substituted bismuth ferrite thin films, Molecules 27, 7565 (2022). https://doi.org/10.3390/molecules27217565

[71] S. Ramazanov, D. Sobola, Ş. Ţălu, F. Orudzev, A. Arman, P. Kaspar, R. Dallaev, G. Ramazanov, Multiferroic behavior of the functionalized surface of a flexible substrate by deposition of Bi_2O_3 and Fe_2O_3, Microsc. Res. Tech. 85, 1300–1310 (2022). https://doi.org/10.1002/jemt.23996

[72] S. Ramazanov, G. Gajiev, Ş. Ţălu, R. S. Matos, H. D. da Fonseca Filho, Additive contribution of multiferroic film and semiconductor substrate from nanotube array to resistive switching, topographic features, Mod. Electron. Mater. 10, 207–216 (2024). https://doi.org/10.3897/j.moem.10.4.136067

[73] J. Grollier, D. Querlioz, K. Y. Camsari, K. Everschor-Sitte, S. Fukami, M. D. Stiles, Neuromorphic spintronics, Nat. Electron. 3, 360–370 (2020). https://doi.org/10.1038/s41928-019-0360-9

[74] N. Nagaosa, Y. Tokura, Topological properties and dynamics of magnetic skyrmions, Nat. Nanotechnol. 8, 899–911 (2013). https://doi.org/10.1038/nnano.2013.243

[75] K. M. Song, J.-S. Jeong, B. Pan, X. Zhang, J. Xia, S. Cha, et al., Skyrmion-based artificial synapses for neuromorphic computing, Nat. Electron. 3, 148–155 (2020). https://doi.org/10.1038/s41928-020-0385-0

[76] Ş. Ţălu, A unified fractal-entropy-manifold framework for multi-modal medical image fusion, HVM Bioflux. 18, 40–52 (2026).

[77] A. Jordan, R. Scholz, P. Wust, H. Fähling, R. Felix, Magnetic fluid hyperthermia (MFH): Cancer treatment with AC magnetic field induced excitation of biocompatible superparamagnetic nanoparticles, J. Magn. Magn. Mater. 201, 413–419 (1999). https://doi.org/10.1016/S0304-8853(99)00088-8

[78] J. Gao, H. Gu, B. Xu, Multifunctional magnetic nanoparticles: Design, synthesis, and biomedical applications, Acc. Chem. Res. 42, 1097–1107 (2009). https://doi.org/10.1021/ar9000026

[79] I. Fernández-Barahona, M. Muñoz-Hernando, J. Ruiz-Cabello, F. Herranz, J. Pellico, Iron oxide nanoparticles: An alternative for positive contrast in magnetic resonance imaging, Inorganics 8, 28 (2020). https://doi.org/10.3390/inorganics8040028

[80] D. Zhang, J. Zhang, X. Bian, P. Zhang, W. Wu, X. Zuo, Iron oxide nanoparticle-based T_1 contrast agents for magnetic resonance imaging: A review, Nanomaterials 15, 33 (2025). https://doi.org/10.3390/nano15010033

[81] C. Sun, J. S. H. Lee, M. Zhang, Magnetic nanoparticles in MR imaging and drug delivery, Adv. Drug Deliv. Rev. 60, 1252–1265 (2008). https://doi.org/10.1016/j.addr.2008.03.018

[82] N. Malhotra, J.-S. Lee, R. A. D. Liman, J. M. S. Ruallo, O. B. Villaflores, T.-R. Ger, C.-D. Hsiao, Potential toxicity of iron oxide magnetic nanoparticles: A review, Molecules 25, 3159 (2020). https://doi.org/10.3390/molecules25143159

[83] V. Polshettiwar, R. Luque, A. Fihri, H. Zhu, M. Bouhrara, J.-M. Basset, Magnetically recoverable nanocatalysts, Chem. Rev. 111, 3036–3075 (2011). https://doi.org/10.1021/cr100230z

[84] V. K. Pecharsky, K. A. Gschneidner Jr., Giant magnetocaloric effect in $Gd_5(Si_2Ge_2)$, Phys. Rev. Lett. 78, 4494–4497 (1997). https://doi.org/10.1103/PhysRevLett.78.4494

[85] O. Gutfleisch, M. A. Willard, E. Brück, C. H. Chen, S. G. Sankar, J. P. Liu, Magnetic materials and devices for the 21st century: Stronger, lighter, and more energy efficient, Adv. Mater. 23, 821–842 (2011). https://doi.org/10.1002/adma.201002180

[86] A. Smith, C. R. H. Bahl, R. Bjørk, K. Engelbrecht, K. K. Nielsen, N. Pryds, Materials challenges for high performance magnetocaloric refrigeration devices, Adv. Energy Mater. 2, 1288–1318 (2012). https://doi.org/10.1002/aenm.201200167

[87] A. Kitanovski, Energy applications of magnetocaloric materials, Adv. Energy Mater. 10, 1903741 (2020). https://doi.org/10.1002/aenm.201903741